Analysis of ceramic thickness shear piezoelectric gyroscopes

J. S. Yang
Department of Engineering Mechanics, University of Nebraska, Lincoln, Nebraska 68588

(Received 16 September 1996; accepted for publication 19 August 1997)

Equations for linear piezoelectricity are formulated in a reference frame rotating at a constant angular velocity and are simplified by a perturbation procedure when the angular velocity of the reference frame is small. The equations thus obtained are then employed in the analysis of a rectangular ceramic plate piezoelectric gyroscope operating with thickness shear modes. Approximate analytical solutions to the equations resulted from the perturbation procedure are obtained based on Mindlin's two-dimensional equations for a piezoelectric plate which are simplified by the thickness shear long wave approximation. Free-vibration frequencies and mode shapes, as well as the condition for double resonance, are obtained. Forced vibration is also studied which leads to a simple expression for the voltage sensitivity of the gyroscope. The analysis is approximate and qualitative mainly with the purpose of exhibiting some most basic characteristics of the gyroscope. Some of the results are compared with finite element numerical method. © *1997 Acoustical Society of America.* [S0001-4966(97)01812-2]

PACS numbers: 43.40.Yq, 43.38.Fx [PJR]

INTRODUCTION

Piezoelectric materials can be used to make gyroscopes (angular rate sensors)[1] to measure the angular velocity of a rotating body. Piezoelectric gyroscopes can be made of quartz or ceramics.[2] They make use of two modes of a vibrating piezoelectric body in which material particles move in perpendicular directions and the natural frequencies of the two modes must be very close. Examples are flexure–flexure vibrations of beams and thickness shear–thickness shear vibrations of plates.[2]

When a piezoelectric gyroscope is used to measure the angular velocity Ω of a rotating body, the gyroscope is attached to the rotating body and is excited into mechanical vibration by applied alternating voltage through piezoelectric coupling. Then, in the reference frame attached to the rotating body, Coriolis force causes the gyroscope to vibrate in the direction perpendicular to the piezoelectrically excited motion. This motion caused by Coriolis force is related to Ω and can be used to detect it. In the rotating reference frame, piezoelectric gyroscopes undergo small vibrations. The governing equations are more complicated than the equations of linear piezoelectricity in an inertial frame because of Coriolis force terms. These equations can be analyzed analytically or numerically. A numerical analysis can usually give quick and accurate results for gyroscopes working with low-frequency vibration modes like the flexure of beams. However, for high-frequency modes like the thickness shear of plates finite element numerical analysis is difficult and remains a challenging problem.[3] For gyroscopes of regular geometry, analytical analysis is possible which provides more insight into the problem and results can be used to compare with numerical analysis. For beam piezoelectric gyroscopes in flexure both numerical[4,5] and analytical[6–8] results are available. For plate thickness shear gyroscopes, only finite element numerical results from a supercomputer are available.[9] Therefore it is purposeful to perform some analytical analysis on plate thickness shear gyroscopes for a better understanding of the problem.

In this work, a perturbation procedure is established for the equations of linear piezoelectricity in a rotating frame when the angular velocity of the rotating frame is small. The perturbation procedure breaks the time harmonic motion of the piezoelectric body into two steps. In the first step the piezoelectric body behaves as if the reference frame were not rotating. In the second step the motion of the piezoelectric body is driven by Coriolis force corresponding to the motion obtained in the first step. Based on the equations resulting from the perturbation procedure, an approximate analytical analysis is performed on a rectangular ceramic plate gyroscope operating with thickness shear modes. Mindlin's equations for a piezoelectric plate[10] are employed with the thickness shear long wave approximation.[11] Resonant frequencies, mode shapes, double resonance condition, output sensing signal, and voltage sensitivity are obtained which are important in the design of the gyroscope. Some of the analytical results are compared with finite element numerical method.

I. EQUATIONS FOR A PIEZOELECTRIC BODY IN A ROTATING FRAME

Let the piezoelectric body rotate at a constant angular velocity Ω. A reference frame is attached to the body and rotated with it. We study the small vibration of the body in the rotating reference frame. Let the region occupied by the piezoelectric body in the rotating frame be denoted by V and its boundary surface by S with unit outward normal n_i and the following partitions (Fig. 1):

$$S = S_u \cup S_T = S_\phi^f \cup S_\phi^s \cup S_D, \tag{1a}$$

$$\varnothing = S_u \cap S_T = S_\phi^f \cap S_\phi^s = S_\phi^f \cap S_D = S_\phi^s \cap S_D, \tag{1b}$$

where S_u is the part of the surface S on which the mechanical displacement is prescribed and S_T the part of S where the traction vector is prescribed. Here, S_ϕ^f represents the forcing

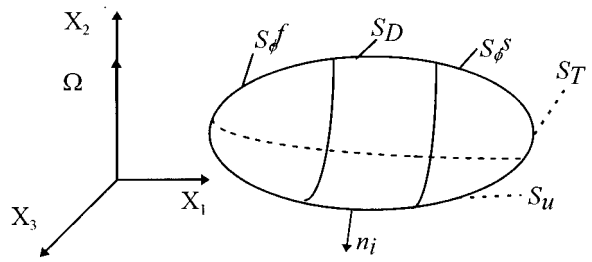

FIG. 1. A piezoelectric body in a rotating reference frame.

electrodes on which known values of the electric potential or voltage is applied and S_ϕ^s represents the sensing electrodes on which values of the electric potential are unknown constants (may be functions of time). We note that S_ϕ^f or S_ϕ^s may each have several disjoint parts with different values of the electric potential on each individual part. S_D is the unelectroded part of the surface. Without loss of generality we orient the x_2 axis along the axis of rotation. The angular velocity vector is represented by $\Omega_j=\Omega \mathfrak{s}_j$, where $(\mathfrak{s}_1,\mathfrak{s}_2,\mathfrak{s}_3)=(0,1,0)$ is the unit vector along the rotation axis. Then the equations of balance of linear momentum for a linear piezoelectric body in the rotating frame can be obtained from the equations for linear piezoelectricity in an inertial frame[11] by adding Coriolis and centrifugal forces as

$$T_{ji,j}+\rho[f_i-2\epsilon_{ijk}\Omega\zeta_j\dot{u}_k+O(\Omega^2)]=\rho\ddot{u}_i \text{ in } V, \tag{2}$$

where u_i is the mechanical displacement vector, T_{ij} the stress tensor, ϵ_{ijk} the permutation tensor, ρ the mass density, and f_i the ordinary body force. The term that is linear in Ω is the Coriolis force which is responsible for the detection of Ω for piezoelectric gyroscopes. $O(\Omega^2)$ is the centrifugal force which is proportional to the square of Ω and the detailed expression of which is not shown because it will be neglected later within the approximation of this analysis. Summation convention for repeated tensor indices and the convention that a comma followed by an index denotes partial differentiation with respect to the coordinate associated with the index are used. A superimposed dot represents the time derivative. The equations of electrostatics, piezoelectric constitutive relations, the strain-displacement, and electric field-potential relations remain the same as those in an inertial frame[11]

$$D_{i,i}=0 \text{ in } V, \tag{3a}$$

$$T_{ij}=c_{ijkl}S_{kl}-e_{kij}E_k \text{ in } V, \tag{3b}$$

$$D_i=e_{ijk}S_{jk}+\epsilon_{ij}E_j \text{ in } V, \tag{3c}$$

$$S_{ij}=(u_{i,j}+u_{j,i})/2 \text{ in } V, \tag{3d}$$

$$E_i=-\phi_{,i} \text{ in } V, \tag{3e}$$

$$u_i=\overline{u_i} \text{ on } S_u, \tag{3f}$$

$$T_{ji}n_j=\overline{t_i} \text{ on } S_T, \tag{3g}$$

$$\phi=\overline{V} \text{ on } S_\phi^f, \tag{3h}$$

$$\phi=\overline{\phi} \text{ on } S_\phi^s, \tag{3i}$$

$$D_i n_i=\overline{d} \text{ on } S_D, \tag{3j}$$

where we have included appropriate boundary conditions (3f)–(3j). In Eq. (3) S_{ij} is the strain tensor, E_i the electric field, D_i the electric displacement, ϕ the electric potential, and all quantities are with respect to the rotating frame. c_{ijkl}, e_{kij}, and ϵ_{ij} are the elastic, piezoelectric, and dielectric constants, respectively. Barred quantities are boundary data which are assumed known, except the values of the electric potential ϕ on the sensing electrodes S_ϕ^s. Since ϕ is unknown on the sensing electrodes, some circuit condition joining the sensing electrodes is needed to determine the value of ϕ. The simplest condition is the open circuit condition which will be used in this analysis and will be shown in detail in the analysis of the rectangular ceramic plate piezoelectric gyroscope later. For the particular purpose of this study, we consider the case when there is no body force f_i and all the boundary conditions are homogeneous except those on the electrodes S_ϕ^f and S_ϕ^s. On the forcing electrodes S_ϕ^f the piezoelectric body is forced by a time harmonic voltage

$$\phi=\overline{V}e^{i\omega t}. \tag{4}$$

Then for steady state vibrations the unknowns u_i and ϕ in V as well as ϕ on S_ϕ^s have the same time dependence and the whole set of equations and boundary conditions (2) and (3) reduce to

$$c_{ijkl}u_{k,lj}+e_{kij}\phi_{,kj}+\rho[-2i\omega\epsilon_{ijk}\Omega\zeta_j u_k+O(\Omega^2)] =-\rho\omega^2 u_i \text{ in } V, \tag{5a}$$

$$e_{kij}u_{i,jk}-\epsilon_{ki}\phi_{,ik}=0 \text{ in } V, \tag{5b}$$

$$u_i=0 \text{ on } S_u, \tag{5c}$$

$$(c_{ijkl}u_{k,l}+e_{kij}\phi_{,k})n_j=0 \text{ on } S_T, \tag{5d}$$

$$\phi=\overline{V} \text{ on } S_\phi^f, \tag{5e}$$

$$\phi=\overline{\phi} \text{ on } S_\phi^s, \tag{5f}$$

$$(e_{kij}u_{i,j}-\epsilon_{ki}\phi_{,i})n_k=0 \text{ on } S_D, \tag{5g}$$

where we have made some substitutions and eliminated some intermediate variables. We note that, although the forcing voltage V can be assumed real for simplicity, the unknowns u_i, ϕ, and ϕ are usually complex. The value of ϕ on the sensing electrodes S_ϕ^s depends on the angular velocity Ω of the rotating frame, hence it can be used to measure Ω. Solutions to the above equations can be attempted directly. However, when the angular velocity Ω is small in a sense that will become clear later, a perturbation procedure can be established which simplifies the problem and reveals the sensing mechanism more clearly without losing much accuracy.

II. A PERTURBATION PROCEDURE

When the piezoelectric gyroscope is used to measure the angular velocity of a rotating body, the forcing frequency ω is very close to a resonant frequency of the gyroscope which

is much larger than the angular velocity of the rotating frame or $\omega \gg \Omega$. Hence a small, dimensionless parameter can be introduced as

$$\lambda = \Omega/\omega \ll 1, \tag{6}$$

and with which we have, from Eq. (5a)

$$c_{ijkl}u_{k,lj} + e_{kij}\phi_{,kj} + \rho\omega^2[-2i\lambda\epsilon_{ijk}\zeta_j u_k + O(\lambda^2)] = -\rho\omega^2 u_i. \tag{7}$$

We then expand all the unknowns as

$$u_j = u_j^{(0)} + \lambda u_j^{(1)} + O(\lambda^2), \tag{8a}$$

$$\phi = \phi^{(0)} + \lambda\phi^{(1)} + O(\lambda^2), \tag{8b}$$

$$\overline{\phi} = \overline{\phi}^{(0)} + \lambda\overline{\phi}^{(1)} + O(\lambda^2), \tag{8c}$$

which, when substituted into Eq. (5), leads to the following perturbation problems of successive orders. For the zeroth-order problem we have

$$c_{ijkl}u_{k,lj}^{(0)} + e_{kij}\phi_{,kj}^{(0)} = -\rho\omega^2 u_i^{(0)} \text{ in } V, \tag{9a}$$

$$e_{kij}u_{i,jk}^{(0)} - \epsilon_{ki}\phi_{,ik}^{(0)} = 0 \text{ in } V, \tag{9b}$$

$$u_i^{(0)} = 0 \text{ on } S_u, \tag{9c}$$

$$(c_{ijkl}u_{k,l}^{(0)} + e_{kij}\phi_{,k}^{(0)})n_j = 0 \text{ on } S_T, \tag{9d}$$

$$\phi^{(0)} = \overline{V} \text{ on } S_\phi^f, \tag{9e}$$

$$\phi^{(0)} = \overline{\phi}^{(0)} \text{ on } S_\phi^s, \tag{9f}$$

$$(e_{kij}u_{i,j}^{(0)} - \epsilon_{ki}\phi_{,i}^{(0)})n_k = 0 \text{ on } S_D. \tag{9g}$$

The zeroth-order problem is the forcing problem. It is seen that the zeroth-order problem does not have the effect of Ω. The piezoelectric body is forced into a time harmonic motion by the applied voltage on S_ϕ^f. The forcing frequency ω should be close to a particular resonant frequency ω_f at which resonance of the forced motion occurs for effective forcing. We note that in this forced vibration without Ω there still may be an output $\overline{\phi}^{(0)}$ on the sensing electrodes S_ϕ^s. This output is not related to Ω and it can usually be eliminated by a proper choice of material orientation, resonant mode of ω_f, or positions and connections of the sensing electrodes. When $\overline{V}$ is real, the zeroth-order response can also be written in real form. For the first-order problem we have

$$c_{ijkl}u_{k,lj}^{(1)} + e_{kij}\phi_{,kj}^{(1)} - \rho\omega^2 2i\epsilon_{ijk}\zeta_j u_k^{(0)} = -\rho\omega^2 u_i^{(1)} \text{ in } V, \tag{10a}$$

$$e_{kij}u_{i,jk}^{(1)} - \epsilon_{ki}\phi_{,ik}^{(1)} = 0 \text{ in } V, \tag{10b}$$

$$u_i^{(1)} = 0 \text{ on } S_u, \tag{10c}$$

$$(c_{ijkl}u_{k,l}^{(1)} + e_{kij}\phi_{,k}^{(1)})n_j = 0 \text{ on } S_T, \tag{10d}$$

$$\phi^{(0)} = 0 \text{ on } S_\phi^f, \tag{10e}$$

$$\phi^{(1)} = \overline{\phi}^{(1)} \text{ on } S_\phi^s, \tag{10f}$$

$$(e_{kij}u_{i,j}^{(1)} - \epsilon_{ki}\phi_{,i}^{(1)})n_k = 0 \text{ on } S_D. \tag{10g}$$

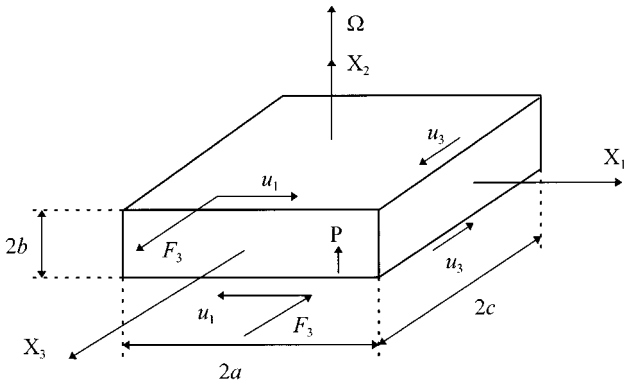

FIG. 2. A rectangular ceramic plate piezoelectric gyroscope.

The first-order problem is the sensing problem. The third term on the left hand side of Eq. (10a) is the Coriolis force due to the zeroth-order motion. The centrifugal force does not show up in the first-order problem because it is of higher order in λ. It can be seen that the first-order motion is driven by the Coriolis force due to the zeroth-order motion. For effective sensing ω should also be close to another resonant frequency ω_S of the piezoelectric body at which resonance of the sensing motion occurs. Hence we must have $\omega \approx \omega_f \approx \omega_s$ which is called double resonance.[5] $\overline{\phi}^{(1)}$ on S_ϕ^s is the quantity that shows the effect of the angular velocity Ω of the reference frame. When the zeroth-order solution is real, the first-order solution can be written in a pure imaginary form.

III. EQUATIONS FOR A CERAMIC PIEZOELECTRIC PLATE

Consider a rectangular ceramic plate poled in the thickness direction as shown in Fig. 2. The plate can vibrate at thickness shear modes. Thickness shear modes are usually coupled with flexural deformations. For a ceramic plate poled in the thickness direction x_2, these thickness shear modes can be excited or detected by lateral electrodes on the sides $x_1 = \pm a$ or $x_3 = \pm c$ of the plate because of the specific forms of the following material constant matrices[12]

$$\begin{pmatrix} c_{11} & c_{13} & c_{12} & 0 & 0 & 0 \\ c_{13} & c_{33} & c_{13} & 0 & 0 & 0 \\ c_{12} & c_{13} & c_{11} & 0 & 0 & 0 \\ 0 & 0 & 0 & c_{44} & 0 & 0 \\ 0 & 0 & 0 & 0 & c_{66} & 0 \\ 0 & 0 & 0 & 0 & 0 & c_{44} \end{pmatrix}, \tag{11a}$$

$$\begin{pmatrix} 0 & 0 & 0 & 0 & 0 & e_{15} \\ e_{31} & e_{33} & e_{31} & 0 & 0 & 0 \\ 0 & 0 & 0 & e_{15} & 0 & 0 \end{pmatrix}, \tag{11b}$$

$$\begin{pmatrix} \epsilon_{11} & 0 & 0 \\ 0 & \epsilon_{33} & 0 \\ 0 & 0 & \epsilon_{11} \end{pmatrix}, \tag{11c}$$

where $c_{66} = (c_{11} - c_{12})/2$. In Eq. (11) the compact matrix notation[11] has been used. c_{pq} and e_{ip} correspond to c_{ijkl} and

e_{ijk} for $p,q=1,...,6$. We note that in Ref. 12 the material matrices are for ceramics poled in the x_3 direction. Here we consider the case of ceramics poled in the x_2 direction whose material matrices can be obtained from the matrices in Ref. 12 by rotating rows and columns properly. Mindlin[10] derived two-dimensional equations for a piezoelectric plate with coupled flexural, thickness shear, thickness twist, and contour (plane stress) modes. For the particular plate in Fig. 2, we exclude contour modes because they will not be excited by lateral electric fields and specialize Mindlin's equations for a ceramic plate as

$$\kappa^2 c_{44}(u^{(0)}_{2,aa}+u^{(1)}_{a,a})+\kappa e_{15}\phi^{(0)}_{,aa}=\rho\ddot{u}^{(0)}_2, \tag{12a}$$

$$\kappa e_{15}(u^{(0)}_{2,aa}+u^{(1)}_{a,a})-\epsilon_{11}\phi^{(0)}_{,aa}=0, \tag{12b}$$

$$\overline{c_{11}}u^{(1)}_{1,11}+c_{66}u^{(1)}_{1,33}+(\overline{c_{13}}+c_{66})u^{(1)}_{3,13}-3b^{-2}\kappa^2 c_{44}(u^{(1)}_1+u^{(0)}_{2,1}) -3b^{-2}\kappa e_{15}\phi^{(0)}_{,1}=\rho\ddot{u}^{(1)}_1, \tag{12c}$$

$$c_{66}u^{(1)}_{3,11}+\overline{c_{11}}u^{(1)}_{3,33}+(\overline{c_{13}}+c_{66})u^{(1)}_{1,13}-3b^{-2}\kappa^2 c_{44}(u^{(1)}_3+u^{(0)}_{2,3}) -3b^{-2}\kappa e_{15}\phi^{(0)}_{,3}=\rho\ddot{u}^{(1)}_3, \tag{12d}$$

where $\phi^{(0)}$, $u^{(0)}_2$, and $u^{(1)}_a$ $(a=1,3)$ are the two-dimensional zeroth-order electric potential, zeroth-order displacement of deflection, and first-order displacements of shear, respectively. They are functions of x_a $(a=1,3)$ and time t. Repeated indices are summed over 1, 3. Equation (12a) is the equation for flexure, Eq. (12b) the equation for electrostatics, and Eqs. (12c) and (12d) the equations for shear. We note that, beginning with this section, superscripts are no longer related to orders of perturbation. They are orders of various quantities in the plate theory. Once the perturbation procedure is understood, it can be carried out without superscripts for perturbation orders. In Eq. (12)

$$\overline{c_{11}}=c_{11}-c^2_{13}/c_{33}, \quad \overline{c_{13}}=c_{12}-c^2_{13}/c_{33}, \tag{13}$$

and

$$\kappa^2=\pi^2/12, \tag{14}$$

is the thickness shear correction factor which is determined by requiring the thickness shear frequencies obtained from the two-dimensional plate equations and the three-dimensional equations to be the same for an infinite ceramic plate. We note that the general two-dimensional equations for piezoelectric plates have two correction factors κ_1 and κ_3 for thickness shears in the x_1 and x_3 directions separately.[10] Since ceramics are transversely isotropic, the two correction factors are equal. To apply boundary conditions, we also need the following:[10]

$$T^{(0)}_{2a}=2b[\kappa^2 c_{44}(u^{(0)}_{2,a}+u^{(1)}_a)+\kappa e_{15}\varphi^{(0)}_{,a}], \tag{15a}$$

$$D^{(0)}_a=2b[\kappa e_{15}(u^{(0)}_{2,a}+u^{(1)}_a)-\epsilon_{11}\phi^{(0)}_{,a}], \tag{15b}$$

$$T^{(1)}_{11}=\tfrac{2}{3}b^3(\overline{c_{11}}u^{(1)}_{1,1}+\overline{c_{13}}u^{(1)}_{3,3}), \tag{15c}$$

$$T^{(1)}_{33}=\tfrac{2}{3}b^3(\overline{c_{13}}u^{(1)}_{1,1}+\overline{c_{11}}u^{(1)}_{3,3}), \tag{15d}$$

$$T^{(1)}_{13}=\tfrac{2}{3}b^3 c_{66}(u^{(1)}_{1,3}+u^{(1)}_{3,1}), \tag{15e}$$

which are the shearing force (15a), zeroth-order electric displacement (15b), bending moment in the x_1 direction (15c), bending moment in the x_3 direction (15d), and twisting moment (15e), respectively. Analytical solutions to the above system of Eqs. (12) can be attempted. However, we will simplify the problem a little more before we proceed to solve it.

IV. THICKNESS SHEAR APPROXIMATION

Thickness shear modes are usually accompanied by weak flexural deformations. This weak flexural deformation can be eliminated by the so called thickness shear approximation which further simplifies the problem. Enlightened by the thickness shear approximation for a system of one-dimensional equations for quartz,[11] we proceed as follows. From Eqs. (12a) and (12b), we obtain, by eliminating $\phi^{(0)}$

$$\kappa^2\left(c_{44}+\frac{e^2_{15}}{\epsilon_{11}}\right)(u^{(0)}_{2,aa}+u^{(1)}_{a,a})=\rho\ddot{u}^{(0)}_2. \tag{16}$$

Substitution of the following wave solution in Eq. (16):

$$u^{(0)}_2=A_2\ \exp[i(\omega t+\xi_a x_a)], \qquad u^{(1)}_b=A_b\ \exp[i(\omega t+\xi_a x_a)], \tag{17}$$

results in the dispersion relation

$$\kappa^2\left(c_{44}+\frac{e^2_{15}}{\epsilon_{11}}\right)(-A_2\xi_a\xi_a+A_a i\xi_a)=-\rho\omega^2 A_2. \tag{18}$$

Since we are interested in long waves with small wave number ξ_a, the term quadratic in ξ_a in the above equation can be dropped. Also, since the frequency ω is very close to the thickness shear frequency of an infinite plate, we make the following substitution in Eq. (18);

$$\omega^2\approx\omega^2_\infty=\frac{\pi^2 c_{44}}{4\rho b}, \tag{19}$$

where ω_∞ is the infinite plate thickness shear frequency. This leads to the simplified dispersion relation

$$A_2=-\frac{b^2}{3}\left(1+\frac{e^2_{15}}{c_{44}\epsilon_{11}}\right)i\xi_a A_a, \tag{20}$$

which is equivalent to the differential relation

$$u^{(0)}_2=-\frac{b^2}{3}(1+k^2_{15})u^{(1)}_{a,a}, \tag{21}$$

where we have denoted

$$k^2_{15}=\frac{e^2_{15}}{c_{44}\epsilon_{11}}. \tag{22}$$

Substituting Eq. (21) into (12c) and (12d), neglecting the $u^{(0)}_2$ term in (12b) under the long wave approximation, we obtain the following equations we need to solve under the thickness shear approximation:

$$\kappa e_{15} u_{a,a}^{(1)} - \epsilon_{11} \phi_{,aa}^{(0)} = 0, \tag{23a}$$

$$c_{11}^* u_{1,11}^{(1)} + c_{66} u_{1,33}^{(1)} + c_{13}^* u_{3,13}^{(1)} - 3b^{-2}\kappa^2 c_{44} u_1^{(1)} - 3b^{-2}\kappa e_{15}\phi_{,1}^{(0)} = \rho \ddot{u}_1^{(1)}, \tag{23b}$$

$$c_{66} u_{3,11}^{(1)} + c_{11}^* u_{3,33}^{(1)} + c_{13}^* u_{1,13}^{(1)} - 3b^{-2}\kappa^2 c_{44} u_3^{(1)} - 3b^{-2}\kappa e_{15}\phi_{,3}^{(0)} = \rho \ddot{u}_3^{(1)}, \tag{23c}$$

where

$$c_{11}^* = \overline{c_{11}} + \kappa^2 c_{44}(1 + k_{15}^2), \tag{24a}$$

$$c_{13}^* = \overline{c_{13}} + c_{66} + \kappa^2 c_{44}(1 + k_{15}^2). \tag{24b}$$

Once $u_a^{(1)}$ are known, $u_2^{(0)}$ can be obtained through Eq. (21). Corresponding to Eqs. (15a) and (15b), under the thickness shear approximation, we have

$$T_{2a}^{(0)} = 2b(\kappa^2 c_{44} u_a^{(1)} + \kappa e_{15}\varphi_{,a}^{(0)}), \tag{25a}$$

$$D_a^{(0)} = 2b(\kappa e_{15} u_a^{(1)} - \epsilon_{11}\phi_{,a}^{(0)}), \tag{25b}$$

which are useful when specifying boundary conditions for Eq. (23). Equations (15c)–(15e) remain the same under thickness shear approximation. We note that the infinite plate thickness shear frequency ω_∞ may have more than one value depending on whether the edges at infinity are shorted or open. This difference is neglected in the present analysis.

V. DRIVING IN THE X_1 DIRECTION

Thickness shear in the x_1 direction can be driven by a voltage $2V_1$ applied across a pair of electrodes ate $x_1 = \pm a$. Since the main motion is $u_1^{(1)}$, we neglect $u_3^{(1)}$ and the small variation along x_3. Then from Eqs. (23a), (23b), and (25a) we have

$$\kappa e_{15} u_{1,1}^{(1)} - \epsilon_{11}\phi_{,11}^{(0)} = 0, \quad -a < x_1 < a, \tag{26a}$$

$$c_{11}^* u_{1,11}^{(1)} - 3b^{-2}\kappa^2 c_{44} u_1^{(1)} - 3b^{-2}\kappa e_{15}\phi_{,1}^{(0)} = \rho \ddot{u}_1^{(1)}, \quad -a < x_1 < a, \tag{26b}$$

$$T_{21}^{(0)} = 2b(\kappa^2 c_{44} u_1^{(1)} + \kappa e_{15}\varphi_{,1}^{(0)}) = 0, \quad x_1 = \pm a, \tag{26c}$$

$$\phi^{(0)} = \pm V_1 \sin \omega t, \quad x_1 = \pm a. \tag{26d}$$

Equation (26c) physically represents free edges at $x_1 = \pm a$. As an approximation, we neglect the piezoelectric coupling term to $u_1^{(1)}$ in the electrostatic equation (26a). We still keep the piezoelectric coupling term to $\phi^{(0)}$ in Eq. (26b). Once $\phi^{(0)}$ is obtained approximately from Eq. (26a) by neglecting the piezoelectric coupling term in Eq. (26a), it is substituted into Eq. (26b) through the piezoelectric coupling term in Eq. (26b). This type of approximation of neglecting piezoelectric coupling at certain places is common in piezoelectric analysis.[13] For materials with weak piezoelectric coupling, quartz for example, this approximation causes very little error. For ceramics the piezoelectric coupling is not weak. However, this approximation will not affect the qualitative behavior of the problem which is the purpose of this paper. Under this approximation, we obtain the approximate solution of the driving electric potential as

$$\phi^{(0)} = \frac{x_1}{a} V_1 \sin \omega t \approx \frac{8}{\pi^2} V_1 \sin \frac{\pi x_1}{2a} \sin \omega t, \tag{27}$$

which satisfies the electric boundary condition (26d). Note that in Eq. (27) we have approximated a linear function of x_1 over $[-a,a]$ by a sine function. It can be considered as a one term approximation by Fourier series. Substituting Eq. (27) into (26b), we then obtain the following expression for $u_1^{(1)}$:

$$u_1^{(1)} = B_1 \cos \frac{\pi x_1}{2a} \sin \omega t, \tag{28}$$

where

$$B_1 = \frac{2\sqrt{3}}{\omega^2 - \omega_\infty^2(1 + c_{11}^* b^2/c_{44}a^2)} \frac{e_{15} V_1/a}{\rho b^2}. \tag{29}$$

We note that the mechanical boundary conditions (26c) are satisfied approximately because $u_1^{(1)}(x_1 = \pm a) = 0$ from Eq. (28).

VI. SENSING IN THE X_3 DIRECTION

With the driving solution $u_1^{(1)}$ known, we have the displacement field

$$u_1 = x_2 u_1^{(1)} = B_1 x_2 \cos \frac{\pi x_1}{2a} \sin \omega t, \tag{30}$$

which leads to a Coriolis force field

$$\mathbf{F} = -2\Omega \mathbf{e}_2 \times \dot{u}_1 \mathbf{e}_1 = 2\Omega \dot{u}_1 \mathbf{e}_3, \tag{31}$$

or

$$F_3 = 2\Omega \omega B_1 x_2 \cos \frac{\pi x_1}{2a} \cos \omega t \approx \frac{4}{\pi} \Omega \omega B_1 x_2 \cos \omega t \approx 2\Omega \omega B_1 x_2 \cos \frac{\pi x_3}{2c} \cos \omega t, \tag{32}$$

where we have approximated a cosine function over $[-a,a]$ by a constant, and similarly a constant over $[-c,c]$ by a cosine function. To apply the Coriolis force in the plate equations, we need to find the following quantity[10]

$$F_3^{(1)} = \int_{-b}^{b} x_2 F_3 \, dx_2 = \frac{2b^3}{3} 2\Omega \omega B_1 \cos \frac{\pi x_3}{2c} \cos \omega t. \tag{33}$$

Then from Eqs. (23a), (23c), and (25), with (33), we have the following sensing problem

$$c_{11}^* u_{3,33}^{(1)} - 3b^{-2}\kappa^2 c_{44} u_3^{(1)} - 3b^{-2}\kappa e_{15}\phi_{,3}^{(0)} + \frac{3}{2b^3}\rho F_3^{(1)} = \rho \ddot{u}_3^{(1)}, \quad -c < x_3 < c, \tag{34a}$$

$$\kappa e_{15} u_{3,3}^{(1)} - \epsilon_{11}\phi_{,33}^{(0)} = 0, \quad -c < x_3 < c, \tag{34b}$$

$$T_{23}^{(0)} = 2b(\kappa^2 c_{44} u_3^{(1)} + \kappa e_{15}\varphi_{,3}^{(0)}) = 0, \quad x_3 = \pm c, \tag{34c}$$

$$\phi^{(0)} = \pm V_3 \cos \omega t, \quad x_3 = \pm c, \tag{34d}$$

$$D_3^{(0)} = 2b(\kappa e_{15} u_3^{(1)} - \epsilon_{11}\varphi_{,3}^{(0)}) = 0, \quad x_3 = \pm c, \tag{34e}$$

where, since the sensing motion is $u_3^{(1)}$, we have neglected $u_1^{(1)}$ and the small variation along x_1. Equation (34c) physically represents free edges at $x_3=\pm c$. We note that in Eq. (34), since V_3 is unknown, we need some circuit condition joining the sensing electrodes to determine V_3. We consider the simple case of open circuit in which $D_3^{(0)}$ or the charge and hence the current on the sensing electrodes vanish in Eq. (34e). As an approximation, we neglect the piezoelectric coupling term to $\phi^{(0)}$ in Eq. (34a) while keeping the piezoelectric coupling term to $u_3^{(1)}$ in Eq. (34b). Then, under the driving of the Coriolis force $F_3^{(1)}$, we obtain, from Eq. (34a),

$$u_3^{(1)}=B_3\cos\frac{\pi x_3}{2c}\cos\omega t, \tag{35}$$

where

$$B_3=\frac{-2\Omega\omega}{\omega^2-\omega_\infty^2(1+c_{11}^*b^2/c_{44}c^2)}B_1. \tag{36}$$

With $u_3^{(1)}$ known, from Eq. (34b), we obtain

$$\phi^{(0)}=A_3\sin\frac{\pi x_3}{2c}\cos\omega t\approx\frac{\pi^2}{8}A_3\frac{x_3}{c}\cos\omega t, \tag{37}$$

where

$$A_3=\frac{ce_{15}}{\sqrt{3}\epsilon_{11}}B_3, \tag{38}$$

and we note that the mechanical boundary conditions (34c) and the open circuit condition (34e) are satisfied because $u_3^{(1)}(x_3=\pm c)=0$ and $\phi_{,3}^{(0)}(x_3=\pm c)=0$ from Eqs. (35) and (37). The electric boundary condition (34d) will give the sensing voltage, as shown in the next section.

VII. DISCUSSION

From Eqs. (37), (34d), (29), (36), and (38), the sensing voltage is

$$\begin{aligned}V_3&=\phi^{(0)}(x_3=c)\\&=\left[\frac{\pi^2ce_{15}}{8\sqrt{3}\epsilon_{11}}\right]\left[\frac{-2\Omega\omega}{\omega^2-\omega_\infty^2(1+c_{11}^*b^2/c_{44}c^2)}\right]\\&\quad\times\left[\frac{2\sqrt{3}}{\omega^2-\omega_\infty^2(1+c_{11}^*b^2/c_{44}a^2)}\frac{e_{15}V_1/a}{\rho b^2}\right]\cos\omega t,\end{aligned} \tag{39}$$

or, for voltage sensitivity

$$\begin{aligned}\frac{V_3}{V_1\Omega}&=\left[-2k_{15}^2\frac{c}{a}\right]\left[\frac{\omega}{\omega^2-\omega_\infty^2(1+c_{11}^*b^2/c_{44}c^2)}\right]\\&\quad\times\left[\frac{\omega_\infty^2}{\omega^2-\omega_\infty^2(1+c_{11}^*b^2/c_{44}a^2)}\right]\cos\omega t,\end{aligned} \tag{40}$$

where

$$\begin{aligned}&c_{11}^*=\overline{c_{11}}+\kappa^2c_{44}(1+k_{15}^2),\quad \overline{c_{11}}=c_{11}-c_{13}^2/c_{33},\\&\kappa^2=\frac{\pi^2}{12},\quad k_{15}^2=\frac{e_{15}^2}{c_{44}\epsilon_{11}},\quad \omega_\infty^2=\frac{\pi^2c_{44}}{4\rho b^2}.\end{aligned} \tag{41}$$

In Eq. (39), the three pairs of brackets on the right hand side represent, from right to left, respectively, the driving of the thickness shear motion in the x_1 direction by the applied voltage V_1 in the x_1 direction, the driving of the thickness shear motion in the x_3 direction by the Coriolis force due to the thickness shear motion in the x_1 direction, and the sensing of the thickness shear motion in the x_3 direction. Roles of various material constants and geometric parameters are clearly exhibited. At resonant frequencies of the sensor, the above expressions become singular. This singularity will disappear when damping is included in the analysis. We note that the forcing voltage is a sine function of time while the sensing voltage is a cosine function. Hence a phase shift is involved. This is because that the Coriolis force, being proportional to the particle velocity, appears like a damping term which causes phase shift although it in fact does no work here since it is perpendicular to the particle velocity. In Eq. (40), the driving dimension a and the sensing dimension c appear in the form of a ratio c/a. Hence the sensitivity depends on the length to width ratio but not the absolute size of the gyroscope. This implies that miniaturization does not lead to lower sensitivity. It is important to note that the driving dimension a is in the denominator and the sensing dimension c is in the numerator in Eq. (40). Therefore better sensitivity can be expected if a gyroscope is designed to be driven at the smaller dimension (plate thickness, for example) and to sense at the larger dimension (plate length or width). The quartz plate thickness shear gyroscope in Ref. 9 has this advantage. From Eq. (40) it can be seen that for large voltage sensitivity the driving frequency and the two natural frequencies of the thickness shear motions in two directions must all be very close. This is the condition of double resonance[5] which implies, from Eq. (39) or (40), that a must be very close to c and the plate is almost square. When that is the case, we can write

$$\omega_\infty^2\left(1+\frac{c_{11}^*b^2}{c_{44}a^2}\right)\approx\omega+\Delta\omega_1, \tag{42a}$$

$$\omega_\infty^2\left(1+\frac{c_{11}^*b^2}{c_{44}c^2}\right)\approx\omega+\Delta\omega_3, \tag{42b}$$

which implies

$$\frac{V_3}{V_1\Omega}\approx-\frac{k_{15}^2}{2}\frac{\omega}{(\Delta\omega_1)(\Delta\omega_3)}. \tag{43}$$

Equation (43) is very simple and it shows that materials with larger electromechanical coupling coefficients (k_{15} here) give higher sensitivity. The commonly used quartz is not a good material in this respect. Equation (43) also shows that the sensitivity is linear in ω. This is natural because from Eq. (32) it can be seen that the Coriolis force, through which the gyroscope is measuring the rotation, is linear in ω. Thickness shear modes have a nodal central plane at $x_2=0$ where the gyroscope can be mounted. Some contouring (variable thickness) may also be considered so that the vibration will be confined in the central portion of the plate because of the energy trapping[14] phenomenon related to thickness shear modes. Then the gyroscope can be supported any where on the edges without affecting its performance. Although the main purpose of the above approximate analysis is to present some qualitative results for the gyroscope, we will compare

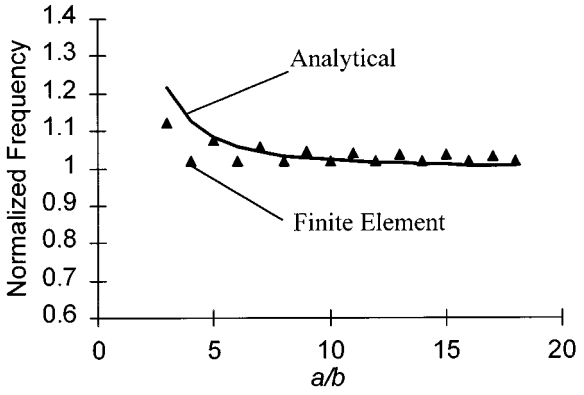

FIG. 3. Normalized thickness shear resonant frequency ω/ω_∞.

the resonant frequencies predicted by the analytical analysis with finite element numerical analysis. Consider a gyroscope made of PZT-5H. We have[12]

$$
\begin{aligned}
&c_{11}=12.6, \quad c_{33}=11.7, \quad c_{44}=2.30,\\
&c_{12}=7.95, \quad c_{13}=8.41\times 10^{10}\ \text{N/m}^2,\\
&c_{66}=(c_{11}-c_{12})/2,\\
&e_{15}=17.0, \quad e_{31}=-6.5, \quad e_{33}=23.3\ \text{C/m}^2,\\
&\epsilon^s_{11}=1700\epsilon_0, \quad \epsilon^s_{33}=1470\epsilon_0,\\
&\epsilon_0=8.854\times 10^{-12}\text{farads/m}, \quad \rho=7500\ \text{kg/m}^3.
\end{aligned}
\tag{44}
$$

The results of resonant frequencies from the above analytical solution and finite element solution as a function of the length–thickness ratio are shown in Fig. 3. The analytical solution is shown by a curve while the finite element solution is represented by small triangles. The frequencies are normalized by ω_∞. We note that the finite element solution can not be represented by one single curve. The small triangles are in fact points on a family of curves.[15] This detailed structure of the frequency spectra is neglected in the analytical analysis, therefore the analytical solution can be represented by one single curve. The analytical solution is obtained by letting the denominator in Eq. (39) vanish. The finite element analysis is done on a supercomputer under the plane strain assumption because both the driving modes (26) and the sensing modes (34) are essentially plain strain. The two end electrodes are shorted. The two solutions agree very well. They both approach the infinite plate solution with the value of 1 as the aspect ratio a/b becomes very large. When a/b decreases, the difference between the two solutions increases. This is because that for small aspect ratios flexural deformation becomes more important in thickness shear modes. (For an infinite ceramic plate with $a/b=\infty$, the thickness shear mode is pure, without flexural deformation.) While finite element method can take care of this flexural deformation without any additional inaccuracy, the above analytical method can only handle this flexural deformation approximately under the thickness shear approximation. Another reason is that for an infinite ceramic plate the thickness shear mode we have been computing is pure elastic without piezoelectric coupling. For a finite plate, piezoelectric coupling exists and the finite element method takes the piezoelectric coupling into full account but the above analytical method treats the piezoelectric coupling approximately.

VIII. CONCLUSION

Equations for the small vibration of a rotating piezoelectric body are simplified by a perturbation procedure which reveals the mechanism of piezoelectric gyroscopes. It is a general formulation and can be used in conjunction with various numerical and analytical methods for the analysis of beam or plate piezoelectric gyroscopes. The approximate analytical solution on the ceramic plate thickness shear gyroscope given in this work presents some simple results which exhibit the effect of various geometrical and material parameters on the sensitivity of the gyroscope. The two-dimensional equations for piezoelectric plates can be employed effectively in the analysis of plate piezoelectric gyroscopes. These equations can be further simplified by the thickness shear long wave approximation. The present analysis can be performed on thickness shear gyroscopes made of quartz or other materials.

ACKNOWLEDGMENTS

The author would like to thank Dr. J. Mattson of Motorola for a discussion on the perturbation procedure, and Dr. W. Zhang of Motorola for discussions on coupled thickness shear and flexural vibrations of plates.

[1] W. D. Gates, ''Vibrating angular rate sensor may threaten the gyroscope,'' Electronics **41** (10), 130–134 (10 June 1968).
[2] J. Soderkvist, ''Micromachined gyroscopes,'' Sens. Actuators A **43**, 65–71 (1994).
[3] Y.-K. Yong, Z. Zhang, and J. Hou, ''On the accuracy of plate theories for the prediction of unwanted modes near the fundamental thickness shear mode,'' Proc. IEEE Frequency Control Symp. 755–760 (1995).
[4] M. Rodamaker and C. R. Newell, ''Finite element analysis of a quartz angular rate sensor,'' ANSYS Conference Proceedings, 3.35–48 (1989).
[5] S. Kudo, S. Sugawara, and N. Wakatuki, ''Finite element analysis of single crystal tuning forks for gyroscopes,'' Proceedings of the IEEE Frequency Control Symposium, 640–647 (1996).
[6] C. S. Chou, J. W. Yang, Y. C. Huang, and H. J. Yang, ''Analysis on vibrating piezoelectric beam gyroscope,'' Int. J. Appl. Electromagn. Mater. **2**, 227–241 (1991).
[7] J. Soderkvist, ''Piezoelectric beams and vibrating angular rate sensors,'' IEEE Trans. Ultrason. Ferroelectr. Freq. Control **38**, 271–280 (1991).
[8] I. A. Ulitko, ''Mathematical theory of the fork-type wave gyroscope,'' Proceedings of the IEEE Frequency Control Symposium, 786–793 (1995).
[9] G. M. Reese, E. L. Marek, and D. W. Lobitz, ''Three dimensional finite element calculations of an experimental quartz rotation sensor,'' Proceedings of the IEEE Ultrasonics Symposium, pp. 419–422 (1989).
[10] R. D. Mindlin, ''High frequency vibrations of piezoelectric crystal plates,'' Int. J. Solids Struct. **8**, 895–906 (1972).
[11] H. F. Tiersten, *Linear Piezoelectric Plate Vibrations* (Plenum, New York, 1969).
[12] B. A. Auld, *Acoustic Fields and Waves in Solids* (Wiley, New York, 1973), Vol. 1, pp. 357–382.
[13] Y. Kagawa, T. Tsuchiya, and T. Kawashima, ''Finite element simulation of piezoelectric vibrator gyroscopes,'' IEEE Trans. Ultrason. Ferroelectr. Freq. Control **43**, 509–518 (1996).
[14] D. Salt, *Hy-Q Hand Book of Quartz Crystal Devices* (Van Nostrand Reinhold, UK, 1987), pp. 45–62.
[15] R. D. Mindlin and W. J. Spencer, ''Anharmonic, thickness-twist overtones of thickness-shear and flexural vibrations of rectangular, AT-cut quartz plates,'' J. Acoust. Soc. Am. **42**, 1268–1277 (1967).